Journal of Nano- and Electronic Physics
Vol. **18** No 1, 01008(6pp) (2026)

Журнал нано- та електронної фізики
Том **18** № 1, 01008(6cc) (2026)

OPEN ACCESS

REGULAR ARTICLE

Multitaper Spatial Frequency Domain Signal Noise Reduction in Magnetic Resonance Imaging

S.P. Mamotenko, A.V. Netreba*

Faculty of RadioPhysics, Electronics and Computer Systems, Taras Shevchenko National University of Kyiv, 01601 Kyiv, Ukraine

(Received 15 December 2025; revised manuscript received 17 February 2026; published online 25 February 2026)

Medical data, such as MRI scan information is not being recorded directly as images, but is firstly stored in *k*-space, which corresponds to the MRI signal's spatial frequency spectrum. The high-frequency part of this signal is exposed to the noise of biological and nonbiological nature, possibly complicating the interpretation of the medical scan. To mitigate this, noise reduction is traditionally performed by applying different types of filters and windowing functions to the fully processed MRI scans such as T2-weighted images, or by transforming them back to the frequency domain. However, when starting with these types of data, that is specified not for denoising but for its readability to a medical professional, there is a risk of mis-reconstructing the original signal leading to the loss of image's fine details. Recently, an approach called multitaper analysis which utilizes multiple orthogonal windows (tapers) to process the noisy image was highlighted in the scientific literature on the topic. Here we further investigate its denoising capabilities using as a starting material not the ready-to-read MRI scans, but the data containing both phase and magnitude information to form a complex image from which k-space can be obtained, closely replicating the original MR signal acquisition. We assume that the usage of multiple tapers in k-space can potentially reduce bias and variance, resulting in less noise in the spectral estimate. To determine how the type and count of tapers can affect the denoising results, the comparison with the single periodogram and the non-local means filter is made. The results, evaluated using peak signal-to-noise ratio, show that the multitaper method outperforms the two others, while feature similarity index measure metric gives identical values for multitaper and standard periodogram methods, while both being lower values compared to non-local means filter.

Keywords: MRI, Periodogram, Multitaper, Gaussian noise, Fourier transform, Reconstruction, Denoising.

DOI: 10.21272/jnep.18(1).01008 PACS number: 87.57.cm

1. INTRODUCTION

Raw MRI data is typically represented in *k*-space, which corresponds to the spatial frequency spectrum. The center of a *k*-space contains low-frequency components that describe gradual intensity variations, while high-frequency components are located near the Nyquist boundary and are responsible for the fine details and sharp transitions of the final image. Typically, noise that affects MRI is of thermal origin [1], follows a Gaussian distribution and has a white spectrum, meaning that it introduces the same noise variance at all frequencies. With the constant noise variance, signal-to-noise ratio (SNR) appears lower in the high frequency *k*-space region, so the relative contribution of noise there is higher.

Within the image domain, the Wiener-like filtering approach [2-4] is suitable for removing stationary white noise, such as the Gaussian. Other analogous filtering methods are non-local means (NLM) [5, 6] and wavelet thresholding [7]. The letter one reduces the mean squared error (MSE) between noise-free and the estimated signal by averaging similar patches across the image and is known for being a gold standard approach for preserving the fine structures of the image [8]. Despite these filters' efficiency and the continuous development of specific approaches based on them for the denoising of final MRI scans, ultimately these mathematical models remain largely inapplicable for the similar processing of the raw *k*-space signal, on the level of which Gaussian noise originally impacts the data.

In addition to that, recent medical image denoising studies cover topics from nanoparticle-enhanced brain tumor detection to model-based tomographic reconstruction and artifact reduction [9, 10]. However, relevant *k*-space studies focus mainly on reconstructions based on the incompletely sampled *k*-space data or on the numerical simulations of MR image reconstruction [11, 12]. Regarding the mathematical models at the bases of the k-space filtering approaches, the majority of available studies mainly cover the single window filtering [13, 14]. However, in the recent study done by M.J. Prerau at al. [15] they showed that instead of a single taper method, multitaper analysis can be applied by averaging the spectra from multiple DPSS (Discrete Prolate Spheroidal Sequence) tapers, providing better noise suppression and more robust effectiveness estimates. The work by P. P. Mitra and B. Pesaran [16] covers the multitaper analysis used specifically in the MRI signal processing, mainly focusing on time series application in artifact removal.

* Correspondence e-mail: avn@univ.kiev.ua

© 2026 The Author(s). Journal of Nano- and Electronic Physics published by Sumy State University. This article is distributed under the terms and conditions of the Creative Commons Attribution (CC BY) license.

Cite this article as: S.P. Mamotenko et al., *J. Nano- Electron. Phys.* 18 No 1, 01008 (2026) https://doi.org/10.21272/jnep.18(1).01008

Here we propose another multitaper based approach to noise alleviation of complex MR image with added Gaussian noise in the k-space using 2-D Fast Fourier Transform (FFT).

2. RESEARCH METHODS

In spectral analysis, real signals are represented as sums of sinusoids. A single sinusoid is defined by three parameters: frequency ω, amplitude A, and phase φ. Knowledge of these parameters allows for the computation of the sinusoid at any point in time. A sinusoid can be written as the real part of a complex exponential $Ae^{(\omega t+\varphi)}$. The complex amplitude $Ae^{i\varphi}$ is a phasor whose magnitude equals A and whose argument equals φ and according to the Euler's relation:

$$Acos\varphi + iAsin\varphi = Ae^{i\varphi}$$

$Ae^{i\varphi}$ is a phasor that scales a sinusoid and shifts its phase. The standard Fourier transform performs the transition from the time domain into the frequency domain, while the k-space is the transition from time domain into the space domain. The Fourier space variable for frequency ω, is the inverse of time units, such as radians per second or hertz. A Fourier transform of a spatial function yields spatial frequencies with units of radians per meter, denoted by k. For two-dimensional (2-D) space, spatial frequencies are represented by k_x and k_y, corresponding to two axes in frequency space. The complex 2D sinusoid can be written as:

$$f(x,y) = Ae^{i(k_x x+k_y y+\varphi)}$$

An image can be modeled as a 2-D function $f(x,y)$ of space and displayed in grayscale, where large values of f appear bright and small values appear dark. As in one-dimension, $f(x,y)$ can be written as a sum of scaled and phase-shifted 2-D sinusoids. The inverse Fourier transform has the form:

$$f(x,y) = \iint F(k_x,k_y)e^{i(k_x x+k_y y)}dk_x dk_y,$$

where $F(k_x,k_y)$ is the k-space spectrum and each complex value is a phasor that sets the amplitude and phase of the sinusoid with spatial frequency k_x,k_y. Frequencies near the k-space center represent the average brightness and slow intensity variations, so their amplitudes are typically the largest. High spatial frequencies near the k-space edges correspond to rapid changes and fine details, such as sharp boundaries and edges.

A basic method for spectral estimation is the periodogram, which uses the discrete Fourier transform. For a random discrete-time signal $x[n]$, sampled every Δt for $n = 0,\dots,N-1$, the standard periodogram at frequency f is given by [15]:

$$\hat{S}_p(f) = \frac{\Delta t}{N}\left|\sum_{n=0}^{N-1} x[n]e^{-i2\pi nf\Delta t}\right|^2$$

Because the observation is finite, the periodogram is biased and has high variance. Bias appears as spectral leakage, so peaks are smeared across nearby frequencies, and variance makes the estimate noisy. A common way to reduce leakage is to multiply the data by a taper (window) before the transform, for example Hann, Hamming, or Welch windows.

The single-taper periodogram $\hat{S}_{stp}(f)$ at frequency f is:

$$\hat{S}_{stp}(f) = \Delta t\left|\sum_{n=0}^{N-1} w[n]x[n]e^{-i2\pi nf\Delta t}\right|^2,$$

where $w[n]$ is the taper at time index n. A single taper reduces spectral leakage (bias) compared with the standard periodogram, but common windows are not optimal for bias and the variance of the estimate remains high.

Multitaper spectral estimation improves both bias and variance by averaging L tapered spectra from several orthogonal tapers applied to the same data. These tapers are DPSS, which maximize spectral concentration in a chosen bandwidth. For a time–bandwidth product (TW), the number of DPSS tapers is $L \le 2TW-1$ according to Thomson's Multitaper Method [17]. Given a set of L DPSS tapers $\{w^1,\dots,w^L\}$, the multitaper spectral estimate at frequency f is:

$$\hat{S}_{mt}(f) = \frac{1}{L}\sum_{l=1}^{L}\Delta t\left|\sum_{n=0}^{N-1} w^l[n]x[n]e^{-i2\pi nf\Delta t}\right|^2$$

Here $x[n]$, $n = 0,\dots,N-1$, is the discrete-time data sampled with interval Δt. N is the number of samples and $\{w^1,\dots,w^L\}$ are L orthogonal Slepian sequences (DPSS) used as tapers (Fig. 1).

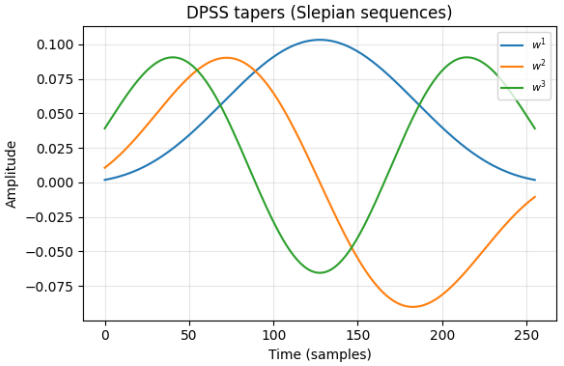

Fig. 1 – First three DPSS tapers (Slepian sequences) w^1, w^2, w^3 of length $N = 256$ for time-bandwidth product $TW = 2$. The first taper is the smoothest, while higher-order tapers exhibit more oscillations

For a 2-D image we extend the one-dimensional multitaper method along both axes. Let $s[n_x,n_y]$ be a real or complex image with $n_x = 0,\dots,N_x-1, n_y = 0,\dots,N_y-1$ and sampling steps $\Delta x,\Delta y$. Along each axis we use one-dimensional DPSS tapers $v_{N_x}^{l_x}[n_x]$ and $v_{N_y}^{l_y}[n_y]$, $l_x = 1,\dots,L_r, l_y = 1,\dots,L_c$. A 2-D taper of order l_x,l_y is the outer product $w^{l_x,l_y}[n_x,n_y] = v_{N_x}^{l_x}[n_x]v_{N_y}^{l_y}[n_y]$, normalized so that $\sum_{n_x n_y}\left|w^{l_x,l_y}[n_x,n_y]\right|^2 = 1$. The tapered spectral estimate $\hat{S}^{l_x,l_y}(k_x,k_y)$ equals:

$$\Delta x\Delta y\left|\sum_{n_x=0}^{N_x-1}\sum_{n_x=0}^{N_y-1} s[n_x,n_y]w^{l_x,l_y}[n_x,n_y]e^{-i(k_x n_x\Delta x+k_y n_y\Delta y}\right|^2,$$

and the 2-D multitaper spectrum is the average over all $L = L_r L_c$tapers:

$$\hat{S}_{mt}^{2D}(k_x, k_y) = \frac{1}{L}\sum_{l=1}^{L_r}\sum_{l=1}^{L_c}\hat{S}^{l_x,l_y}(k_x, k_y)$$

Thus, the 2-D multitaper PSD is the mean of L orthogonal, DPSS-tapered 2-D FFT spectra and this reduces the signal's spectral leakage and variance compared with a single-taper estimate. We assume that the measured complex image $s_{obs}[n_x, n_y] = s[n_x, n_y] + n[n_x, n_y]$ is the sum of an unknown noise-free image s and additive complex Gaussian noise n with zero mean and variance σ^2. Because we use a 2-D Fast Fourier Transform (FFT), the same model holds in k-space:

$$K_{obs}(k_x, k_y) = K_s(k_x, k_y) + N(k_x, k_y),$$

with $N(k_x, k_y)$ is white complex Gaussian noise with a flat power spectrum $S_n(k_x, k_y) = \sigma^2$.

The 2-D multitaper estimator gives a power spectrum $\hat{S}_{mt}^{2D}(k_x, k_y)$ of the noisy image. For a noise-only image the expected value of this spectrum is a constant N_0^{mt} and compute from the known noise variance σ^2. To construct a denoising operator, we follow the classical Wiener filtering formulation [18] for linear MSE estimation. For a stationary process with signal PSD $S_s(f)$ and noise PSD $S_n(f)$, the Wiener filter has frequency response $S_s(f)/(S_s(f) + S_n(f))$. In our setting the true signal PSD S_s is unknown, so we approximate the total spectrum $S_s + S_n$ by $\hat{S}_{mt}^{2D}$ and set $S_n \approx N_0^{mt}$. This leads to the spectral shrinkage gain:

$$G(k_x, k_y) = \max\left\{0, 1 - \frac{N_0^{mt}}{\hat{S}_{mt}^{2D}(k_x, k_y) + \varepsilon}\right\},$$

with $\varepsilon > 0$, a small positive constant added to the denominator to avoid division by zero. The denoised k-space is then $\tilde{K}(k_x, k_y) = G(k_x, k_y)K_{obs}(k_x, k_y)$ and the final complex MR image is obtained by the inverse 2-D FFT of $\tilde{K}$. In all tests, we use the clinical brain MRI data provided by one of the authors containing the separate magnitude and phase DICOM images (Fig. 2), which were combined into a single complex-valued reference image. Working with complex data allows us to model thermal MRI noise as additive complex Gaussian noise directly in k-space.

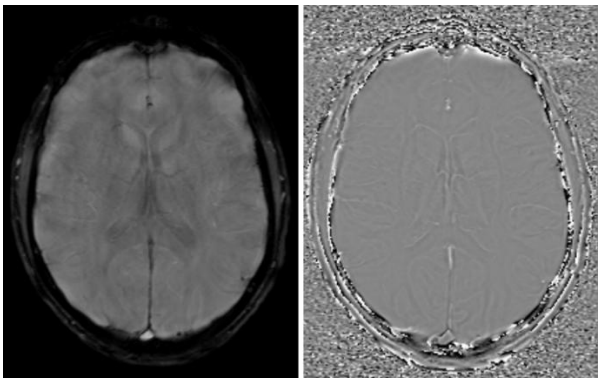

a b

Fig. 2 – Magnitude image (a), phase image (b)

For performance evaluation we use Peak Signal-to-Noise Ratio (PSNR) and the Feature Similarity Index Measure (FSIM). PSNR is a standard signal-based metric that compares a reference image and its noise-contaminated version using the mean squared error; it quantifies reconstruction quality in decibels, with higher values indicating better result. In this study PSNR is computed on the magnitude image within a smooth brain region of interest (ROI) to avoid a bias from the black background. Image quality assessment allows solving a number of applied problems in the signal processing techniques for biological tissues classifying and pathological state diagnosing [19].

FSIM is a metric proposed by Zhang et al. [20] that compares images based on low-level features, primarily phase congruency and gradient magnitude, which are highly correlated with the human visual perception. FSIM values lie in [0, 1], with values closer to 1 indicating higher perceived similarity. We compute FSIM within an edge region of interest (edge ROI) defined by thresholding the gradient magnitude of the reference magnitude image, which focuses the evaluation on preservation of anatomical boundaries and cortical structures of the brain.

3. RESULTS

The proposed method was evaluated on a complex MR head image reconstructed from a magnitude-phase DICOM pair. The main parameters of MR images are as follows: 24-year-old male, axial plane, slice location: − 4.99 mm. Artificial complex Gaussian noise was added in k-space to obtain a target SNR of 10 dB. For each reconstruction, the magnitude image was normalized to [0, 1]. Within the brain, a smooth ROI and an edge ROI were defined by thresholding the gradient magnitude of the clean image. Denoising quality was measured by the peak signal-to-noise ratio in the smooth ROI, and the feature similarity index in the edge ROI, FSIM, averaged over five independent noise realizations.

The time–bandwidth product TW was varied from 2.0 to 8.0. The numbers of DPSS tapers in the readout and phase-encode directions, L_r and L_c, were taken from 2 to 8 under the usual constraint $L = L_r, L_c \leq 2TW - 1$. For each parameter set, the multitaper power spectral density estimate, the analytic noise floor matched to the DPSS tapers, and the resulting Wiener gain were computed as described above.

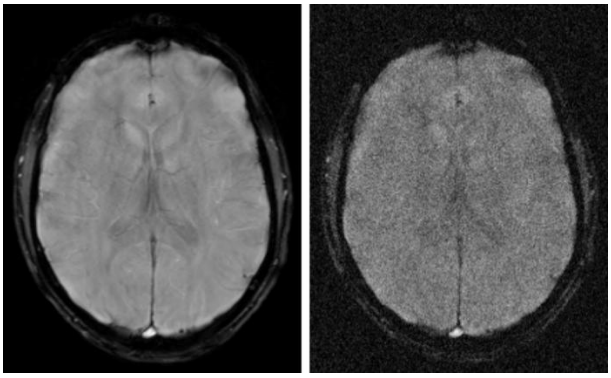

a b

Fig. 3 – Original brain MR image (a), brain MR image with Gaussian noise (b)

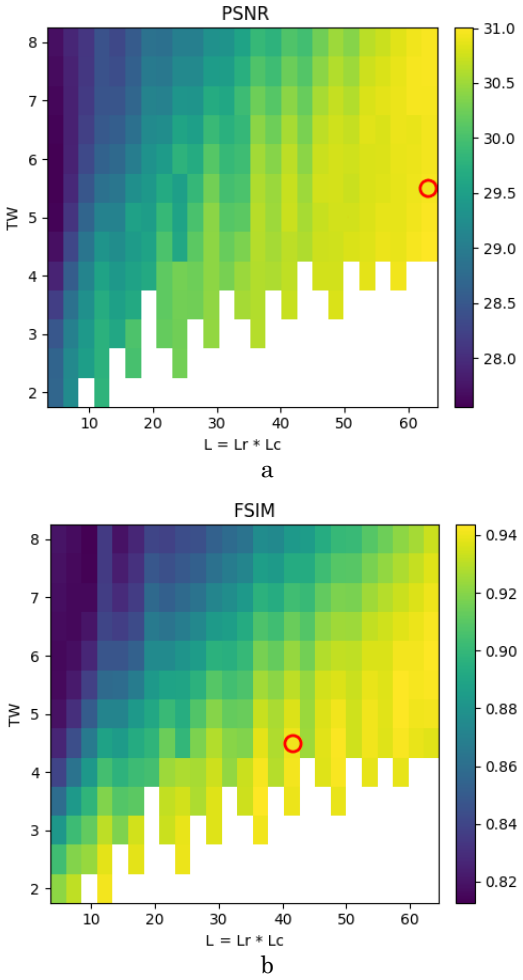

Fig. 4 – Multitaper PSNR heatmap (a), multitaper FSIM heatmap (b); the red circle marks the highest value of the corresponding metric

PSNR tends to increase with the higher values of TW and L (Fig. 4a). The highest PSNR is obtained for $TW = 5.5$ with $L_r = 8$, $L_c = 8$ ($L = 64$), which indicates that the noise level, and thus the PSNR metric, improves when a larger number of tapers is used. However, this leads to excessive smoothing of the MR image. To find a compromise between smoothing and noise reduction, we use the FSIM metric. FSIM reaches its maximum already at $TW = 4.5$ with $L_r = 6$, $L_c = 7$ ($L = 42$) which indicates the best preservation of brain structures for this parameter set. We therefore use the maximum FSIM value as a guideline and reconstruct the denoised image using the corresponding TW and L (Fig. 4b).

The same configuration was then compared with two baseline methods: a standard periodogram-based filter in k-space and a spatial non-local means (NLM) filter, configured as in the study by J.V. Manjón et al. [6] and applied to the noisy magnitude image. In this comparison, the same complex Gaussian noise realization in k-space was used for all three methods in each run (Fig. 4b). The k-space periodogram employed a single rectangular window and the same analytic noise variance as in the multitaper. The NLM filter was applied to the magnitude image normalized to [0,1], with the smoothing parameter estimated from the data. Results for the comparison are as follows:

Table 1 – Quantitative comparison of denoising methods.

Method	PSNR	FSIM
Multitaper	30.82 ± 0.09	0.94 ± 0.001
Periodogram	26.57 ± 0.07	0.94 ± 0.002
NLM	29.66 ± 0.15	0.96 ± 0.001

Table 1 summarizes the mean PSNR and FSIM over five independent runs. Higher PSNR values yielded by the multitaper method reflect stronger noise reduction compared to other methods. FSIM metric results are identical for multitaper and standard periodogram method, while FSIM for NLM shows a 0.02 value increase. Images reconstructed by the multitaper, standard periodogram and NLM methods:

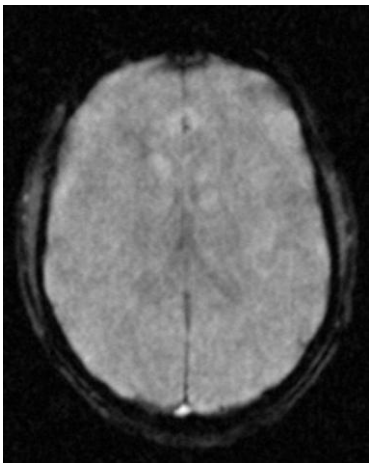

Fig. 5 – Brain MR image denoised with the multitaper method

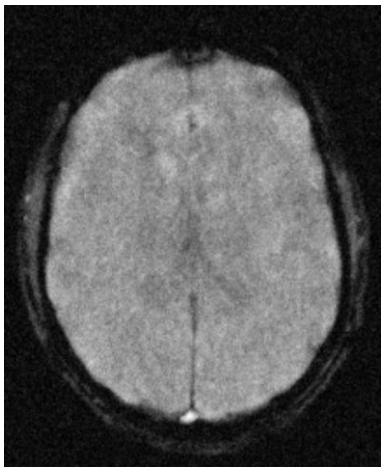

Fig. 6 – Brain MR image denoised with the standard periodogram

Visual perception largely corresponds with the results estimated using PSNR and FSIM, with the authors' personal evaluation being that the multitaper method (Fig. 5) holds an advantage over the standard periodogram (Fig. 6), while the reconstruction by NLM filter shows the highest visual similarity to the original magnitude image (Fig. 7). Therefore, it can be concluded that, although, the multitaper method outperforms some single-taper methods such as the standard periodogram, it still requires further refinement. Future work in that direction may make use of brain masks or tissue ROIs to minimize the background effect or use

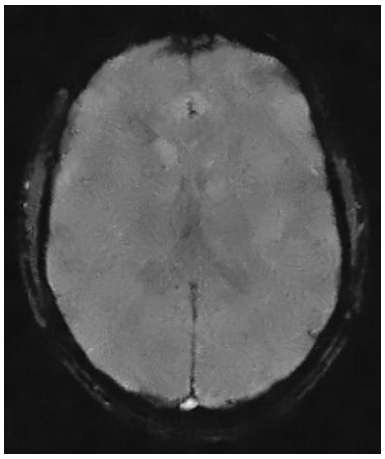

Fig. 7 – Brain MR image denoised with the NLM filter

adaptive selection of *TW* and of the number of tapers based on local image structure. Additionally, approaches combining several MRI denoising methods may lead to the creation of robust reconstruction protocols.

4. CONCLUSIONS

A *k*-space denoising method based on two-dimensional multitaper spectral estimation has been proposed and studied on a real MR brain image with added complex Gaussian noise. The method reconstructs the complex image from real magnitude and phase data, applies a two-dimensional FFT to obtain k-space, and then applies two-dimensional Wiener-like multitaper filtering.

A real brain MR image with both magnitude and phase components was used during the tests. The results show that the multitaper method achieves a higher PSNR than the standard periodogram and the NLM filter, therefore performing noise reduction more effectively compared to the two methods. The FSIM metric for all methods is in the range of 0.94 to 0.96 which is close to the value of 1, indicating that they all reconstruct the image edges to a high extent. The authors note that the NLM filter visually appears superior, as it produces less blurring of brain structures and shows higher perceptive visual similarity to the original image. Still, unlike the multitaper and standard periodogram methods, the NLM filter operates in the image domain rather than in *k*-space and was included as a spatial baseline for the comparison with spectral methods. Noise reduction in *k*-space remains an important topic, since the MRI noise affects the *k*-space information first.

Based on the results of this study we propose that the multitaper method shows clear potential for its application in *k*-space denoising of MR data, however, the topic requires further inquiry. A possible line of work was outlined as such that will focus on tuning the ROIs to reduce the influence of the background, adaptive tuning of the method parameters, and integration with other denoising techniques.

REFERENCES

1. M.S. Hansen, P. Kellman, *J. Magn. Reson. Imaging* **41**, 573 (2015).
2. R. Wirestam, A. Bibic, J. Lätt, S. Brockstedt, F. Ståhlberg, *Magn. Reson. Med.* **56**, 1114 (2006).
3. Y. Zeng, B. Zhang, W. Zhao, S. Xiao, G. Zhang, H. Ren, W. Zhao, Y. Peng, Y. Xiao, Y. Lu, Y. Zong, Y. Ding, *Comp. Math. Methods Med.* **2020**, 1405647 (2020).
4. M. Martin-Fernandez, C. Alberola-Lopez, J. Ruiz-Alzola, C.F. Westin, *Magn. Reson. Imaging* **25**, 278 (2007).
5. A. Sharma, V. Chaurasia, *Signal Image Video Process.* **15**, 1331 (2021).
6. J.V. Manjón, P. Coupé, L. Martí-Bonmatí, D.L. Collins, M. Robles, *J. Magn. Reson. Imaging* **31**, 192 (2010).
7. A. Lanani, A. Abboudi, *J. Nano- Electron. Phys.* **15** No 2, 02023 (2023).
8. J. Mohan, V. Krishnaveni, Y. Guo, *Biomed. Signal Process. Control* **9**, 56 (2014).
9. S. Chandrappa, M.S. Guru Prasad, H.N. NaveenKumar, S. Pachnanda, K.R. Sharath, Ashwini Niteen Yeole, *J. Nano- Electron. Phys.* **16** No 4, 04014 (2024).
10. A. Mondal, D. MItra, A. Dhar, A. Saha, S. Das, P. Ghosh, *J. Nano- Electron. Phys.* **17** No 3, 03008 (2025).
11. A. Netreba, A. Komarov, Y. Kyiashko, I. Pershukov, *Mol. Cryst. Liq. Cryst.* **673**, 97 (2018).
12. A.V. Netreba, Y.O. Kyiashko, *J. Nano- Electron. Phys.* **17** No 3, 03037 (2025).
13. B. Vikhoff-Baaz, G. Starck, M. Ljungberg, K. Lagerstrand, E. Forssell-Aronsson, S. Ekholm, *Magn. Reson. Imaging* **19**, 1227 (2001).
14. A. Kyung, Y.J. Kwon, L. Chung, *2018 9th IEEE Annual Ubiquitous Computing, Electronics & Mobile Communication Conference (UEMCON)*, 742 (New York: IEEE: 2018).
15. M.J. Prerau, R.E. Brown, M.T. Bianchi, J.M. Ellenbogen, P.L. Purdon, *Physiology* **32**, 60 (2017).
16. P.P. Mitra, B. Pesaran, *Biophys. J.* **76**, 691 (1999).
17. S. Karnik, J. Romberg, M.A. Davenport, *IEEE Trans. Inf. Theory* **68**, 4864 (2022).
18. L.-M. Dogariu, J. Benesty, C. Paleologu, S. Ciochină, *Appl. Sci.* **11**, 7774 (2021).
19. Y. Suleimanov, S. Radchenko, O. Lefterov, A. Netreba, S. Vasnyov, V. Sava, J. Sanchez-Ramos, L. Prockop, R. Duara, *IEEE 36th International Conference on Electronics and Nanotechnology (ELNANO 2016)*, art. no. 7493042, 175 (Kyiv: 2016).
20. L. Zhang, L. Zhang, X. Mou, D. Zhang, *IEEE Trans. Image Process.* **20**, 2378 (2011).

Зниження шумової складової сигналу в просторово-частотній області для магнітно-резонансної томографії з використанням багатовіконного методу

С.П. Мамотенко, А.В. Нетреба

Факультет радіофізики, електроніки та комп'ютерних систем, Київський національний університет імені Тараса Шевченка, 01601 Київ, Україна

Медичні дані, якими є безпосередні результати МРТ-обстежень, на початковому етапі реєструються у вигляді сукупності даних, яка відповідає просторовому спектру виміряного сигналу. Високочастотна частина цього сигналу зазнає впливу шумів біологічного й небіологічного походження, що може ускладнювати інтерпретацію медичного зображення. Для зменшення цього впливу шумозниження традиційно виконують шляхом застосування різних типів фільтрів і віконних функцій до фінальних МРТ-зображень, наприклад Т2-зважених, або ж шляхом перетворення їх у частотну область. Однак ці зображення оптимізовані не для шумозниження, а для зручності інтерпретації медичним спеціалістом, тому існує ризик некоректного відновлення початкового сигналу й втрати деталізації зображення. Останнім часом у наукових публікаціях було відмічено підхід багатовіконного аналізу, який використовує кілька ортогональних вікон для обробки зображення з шумом. У цій роботі ми досліджуємо його можливості для шумозниження, використовуючи дані що містять фазову, і амплітудну інформацію, на основі яких формується комплексне зображення, з якого відтворюється k-простір. Ці умови є більш наближеним до реального процесу реєстрації МРТ-сигналу. Ми припускаємо, що використання кількох вікон у k-просторі може зменшити зміщення та дисперсію спектральної оцінки, що призведе до зниження рівня шуму. Щоб визначити, як кількість вікон впливає на ефективність шумозниження, виконано порівняння з одновіконною періодограмою, а також із фільтром Non-Local Means (NLM) – одним із найпоширеніших підходів до шумозниження в медичних зображеннях. Результати, оцінені за піковим співвідношенням сигналу до шуму (PSNR), показують вищі значення для багатовіконного методу, ніж для двох інших. Тоді як індекс подібності ознак (FSIM) дає однакові значення для багатовіконного методу і методу стандартної періодограми, але обидва ці методи поступаються NLM фільтру.

Ключові слова: МРТ, Періодограма, Багатовіконний метод, Ґауссівський шум, Перетворення Фур'є, Реконструкція, Шумозниження.